Solid-State Electronics 229 (2025) 109179

Contents lists available at ScienceDirect

Solid State Electronics

journal homepage: www.elsevier.com/locate/sse

Interlayer exchange coupling for enhanced performance in spin-transfer torque MRAM devices☆

M. Bendra [a,b,*], R.L. de Orio [b], S. Selberherr [b], W. Goes [c], V. Sverdlov [a,b]

[a] Christian Doppler Laboratory for Nonvolatile Magnetoresistive Memory and Logic at the
[b] Institute for Microelectronics, TU Wien, Gußhausstraße 27-29, Wien, A-1040, Austria
[c] Silvaco Europe Ltd., Compass Point, St Ives, Cambridge, PE27 5JL, United Kingdom

ARTICLE INFO

Keywords:
Interlayer exchange coupling
Spin transfer torques
Spin dynamics
Spintronic memory
Multilayer architectures

ABSTRACT

We present a micromagnetic modeling study that explores the impact of interface exchange coupling in multilayered spintronic devices, such as the spin-transfer torque magnetoresistive random access memory, which is at the forefront of nonvolatile storage. By examining the exchange interactions facilitated by non-magnetic or insulating layers between ferromagnetic ones, we explore the critical role of interlayer exchange coupling in the magnetic stability and domain dynamics essential for the efficiency of spin-transfer torque mechanisms. This understanding is crucial for enhancing device performance, particularly in terms of data reliability and access speeds, amid the ongoing miniaturization trend in nanotechnology. The magnetic tunnel junction within spin-transfer torque magnetoresistive random access memory, featuring a CoFeB-based layered structure, enables significant data density improvements through reduced cell sizes and enhanced magnetic properties. However, miniaturization also raises concerns about the reliability and stability of these devices, particularly due to phenomena like back-hopping. Our research addresses these concerns by highlighting the role of IEC in achieving magnetic alignment and optimizing overall device performance, thereby meeting the rigorous requirements of modern memory applications and paving the way for the next generation of memory technologies.

1. Introduction

The emergence of spin-transfer torque magnetoresistive random access memory (STT-MRAM) marks a transformative phase in non-volatile memory technologies, applicable across diverse sectors from Computing-in-Memory architectures [1], automotive systems [2], to real-time industrial settings [3], and high-density memory configurations [4]. Central to STT-MRAM is the magnetic tunnel junction (MTJ), featuring a layered structure with a CoFeB-based reference layer and a free layer, separated by an MgO tunnel barrier (TB) or non-magnetic spacer (NMS). This configuration is crucial for enabling significant data density improvements through miniaturization of memory cells [5].

However, the reduction in cell size raises reliability concerns, notably the back-hopping phenomenon, which jeopardizes memory stability [6,7]. To address these issues, research has focused on the interlayer exchange coupling (IEC) within MTJs, a fundamental aspect for the magnetic alignment and performance of these devices. IEC influences the magnetic alignment of ferromagnetic layers through NMSs or TBs and is critical for tailoring MTJ performance to meet the diverse needs of applications ranging from IoT/AI to automotive and space applications, potentially replacing traditional SRAM, DRAM, and Flash memories [8].

Investigations have also highlighted the evolution of MTJ technology within the CoFeB/MgO material system, characterized by perpendicular magnetic anisotropy and enhanced by interfacial anisotropy modifications such as adding a capping MgO layer or inserting an MgO/NMS layer within the CoFeB free layer [9,10]. These advancements have facilitated the commercialization of MTJs with sub−10 nm dimensions and diameters in the tens of nanometers by semiconductor foundries [11].

Understanding the role of IEC in multilayered structures unveils its crucial impact on magnetic stability and efficiency in spintronic devices, essential for STT switching. This knowledge opens ways for optimizing interlayer exchange coupling to improve data retention and write/read speeds, paving the way for the next generation of memory technologies.

☆ The review of this paper was arranged by Francisco F. Gamiz.

* Corresponding author at: Institute for Microelectronics, TU Wien, Gußhausstraße 27-29, Wien, A-1040, Austria.
E-mail address: bendra@iue.tuwien.ac.at (M. Bendra).

https://doi.org/10.1016/j.sse.2025.109179

Available online 7 July 2025

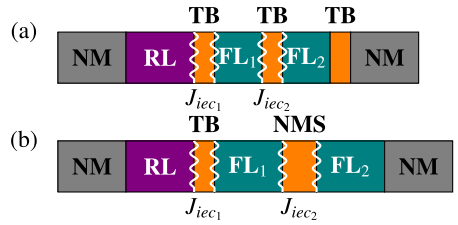

Fig. 1. The intricate design of multilayered MRAM cells in a more comprehensible form. (a) and (b) display an ultra-scaled MRAM cell. Color-coding is utilized for clear differentiation of components. The RL is marked in violet, the FL in green, and the TB or NMS in orange. Non-magnetic (NM) contacts are represented in gray. Interfacial engineering regions are highlighted by white zigzag lines. The interaction strengths between the RL and the first FL (FL_1) and between FL_1 and the second FL (FL_2) are denoted by J_{iec_1} and J_{iec_2}, respectively.

Table 1
Simulation parameters.

LLG Parameters	Stack A	Stack B
Saturation magnetization M_S ($A\,m^{-1}$)	1.2×10^{6}	1.2×10^{6}
Exchange constant A_{exc} ($J\,m^{-1}$)	1.0×10^{-11}	1.0×10^{-11}
Uniaxial anisotropy K_u ($J\,m^{-3}$)		
RL	5.186×10^{5}	5.186×10^{5}
FL_1	8.644×10^{5}	5.186×10^{5}
FL_2	8.644×10^{5}	5.186×10^{5}
Gilbert damping constant α		
RL, FL_1, FL_2	0.015	0.015
Resistance-area product RA_P ($\Omega\,\mu m^2$)	2.4	2.0

2. Micromagnetics model

To enhance the accuracy of micromagnetic models for multilayered MRAM cells, incorporating the IEC precisely is crucial. IEC significantly impacts the functionality of these memory devices by influencing the magnetic interactions between adjacent layers. Our research presents a comprehensive modeling approach which underscores the role of IEC in the context of STT phenomena in MRAM cells.

The MRAM cells, illustrated in Fig. 1, feature a MTJ structure with alternating CoFeB and TB or NMS layers, connected to non-magnetic (NM) contacts, hereafter referred to as Stack A and Stack B. The material properties employed in our simulations are detailed in Table 1 [12,13]. Fig. 1(a) displays an ultra-scaled MRAM cell with a diameter of 2.3 nm. This composite structure consists of CoFeB (5 nm)|MgO (0.9 nm)|CoFeB (3 nm)|MgO (0.9 nm)|CoFeB (3 nm)|MgO (0.9 nm) MTJ connected to NM contacts. In Fig. 1(b), the composite free layer (FL) is separated by a NMS and lacks a capping TB, configured as CoFeB (5 nm)|MgO (0.9 nm)|CoFeB (5 nm)|NMS (2 nm)|CoFeB (3 nm) connected to NM contacts.

Our framework employs the Landau–Lifshitz–Gilbert (LLG) equation to simulate the dynamics of the normalized magnetization, using the finite element method (FEM) for numerical analysis. The implementation utilizes the MFEM library, as documented in [14], with further methodological details provided in [15,16]. The LLG equation is given by:

$$\frac{\partial \mathbf{m}}{\partial t} = -\gamma \mathbf{m} \times \mathbf{H}_{\text{eff}} + \alpha \mathbf{m} \times \frac{\partial \mathbf{m}}{\partial t} + \frac{1}{M_S}\mathbf{T_S} \tag{1}$$

$\mathbf{m}$ is the normalized magnetization vector, M_S the magnetization saturation, γ the gyromagnetic ratio, and α represents the Gilbert damping constant. The effective field $\mathbf{H}_{\text{eff}}$ includes the magnetic anisotropy field, the exchange field, and the demagnetization field. The latter contribution is evaluated only in the disconnected magnetic domain using a hybrid approach which combines the boundary element method (BEM) and the FEM [17]. The spin-transfer torque term $\mathbf{T_S}$ is modeled using a coupled spin and charge drift–diffusion approach which accurately describes the charge and spin transport in magnetic valves [16]. The exchange field originates from quantum mechanical exchange interactions which favor parallel alignment of neighboring magnetic moments. In the micromagnetic framework, this results in an energy term are penalizing spatial variations in magnetization [18]:

$$E_{\text{ex}} = A \int_{\omega} |\nabla \mathbf{m}|^2 \mathrm{d}x \tag{2}$$

ω is the ferromagnetic domain and A the exchange stiffness constant ($J\,m^{-1}$). This represents the lowest-order phenomenological form consistent with the Heisenberg exchange interaction. By applying variational principles, the corresponding exchange field contribution is:

$$\mathbf{H}_{\text{ex}} = \frac{2A}{\mu_0 M_S}\nabla^2 \mathbf{m} \tag{3}$$

The coupling type, such as ferromagnetic (FM) or antiferromagnetic (AFM), corresponds to the band structure around the Fermi surface. For IEC through metallic spacers, the RKKY theory explains the periodic oscillations and rapid decay of coupling strength with spacer thickness, which originates from interactions between localized d- or f-orbit electrons via the conduction electrons [19].

For semiconducting spacers, theories like variable-range hopping and resonant tunneling through defect-induced localized states have been developed. In contrast, for insulating spacers, IEC characterized by significant strength without oscillation is interpreted through spin-dependent tunneling [20].

The free energy density due to interlayer coupling is given by:

$$\mathbf{E} = -J_1 \cos(\Delta\phi) - J_2 \cos^2(\Delta\phi) \tag{4}$$

$\Delta\phi$ represents the angle between the magnetizations of the coupled layers, and J_1 and J_2 describe the nature and strength of the coupling. For an NMS, J_1 shows an oscillatory dependence on the spacer thickness, indicative of RKKY interactions, leading to either FM or AFM coupling based on the spacer thickness. The coupling is predominantly FM for MgO spacers and decays exponentially with the thickness, aligning with the tunneling electron wave function decay.

$J_1 > 0$ signifies FM coupling, promoting parallel (P) magnetizations, while $J_1 < 0$ indicates AFM coupling, favoring an anti-parallel (AP) alignment. The term J_2, often negligible, represents bi-quadratic coupling terms related to non-intrinsic factors like surface roughness [21]. When neglecting J_2, the energy simplifies to:

$$\mathbf{E} = -J_1 \cos(\Delta\phi) \tag{5}$$

Traditionally, IEC has been approximated by an effective bias field acting on the magnetic layers [22], which simplifies its representation, but neglects the angular dependence between the magnetization vectors. This limits the model's ability to accurately capture interfacial coupling effects during dynamic processes such as switching or back-hopping. In micromagnetic modeling, IEC contributions are typically introduced via boundary conditions. However, expressing all energy terms as effective field contributions is often more convenient in dynamic simulations, as it eases integration into the LLG equation [23].

To improve model fidelity, we explicitly incorporate the angular dependence of IEC using boundary terms in the finite element formulation. The corresponding weak-form term is consistent with the framework presented in Equation (36) of [24] and is expressed as:

$$\frac{J_{iec}\gamma}{\mu_0 M_{S,\mathrm{L}}} \int_{R|\text{spacer}} \mathbf{m_L} \cdot \mathbf{w}\,\mathrm{d}x + \frac{J_{iec}\gamma}{\mu_0 M_{S,\mathrm{R}}} \int_{\text{spacer}|L} \mathbf{m_R} \cdot \mathbf{w}\,\mathrm{d}x \tag{6}$$

J_{iec} is the coupling strength, μ_0 the vacuum permeability, $\mathbf{m_L}$ and $\mathbf{m_R}$ the normalized magnetizations of the left and right layers, and $\mathbf{w}$ the test function. This formulation captures the interfacial nature of IEC and enables an accurate evaluation of dynamic coupling in multilayer systems [25].

While the IEC strength J_{iec} strongly depends on the materials and geometry of the MTJ stack, particularly the composition and thickness of the nonmagnetic spacer, the values used in our simulations, ranging

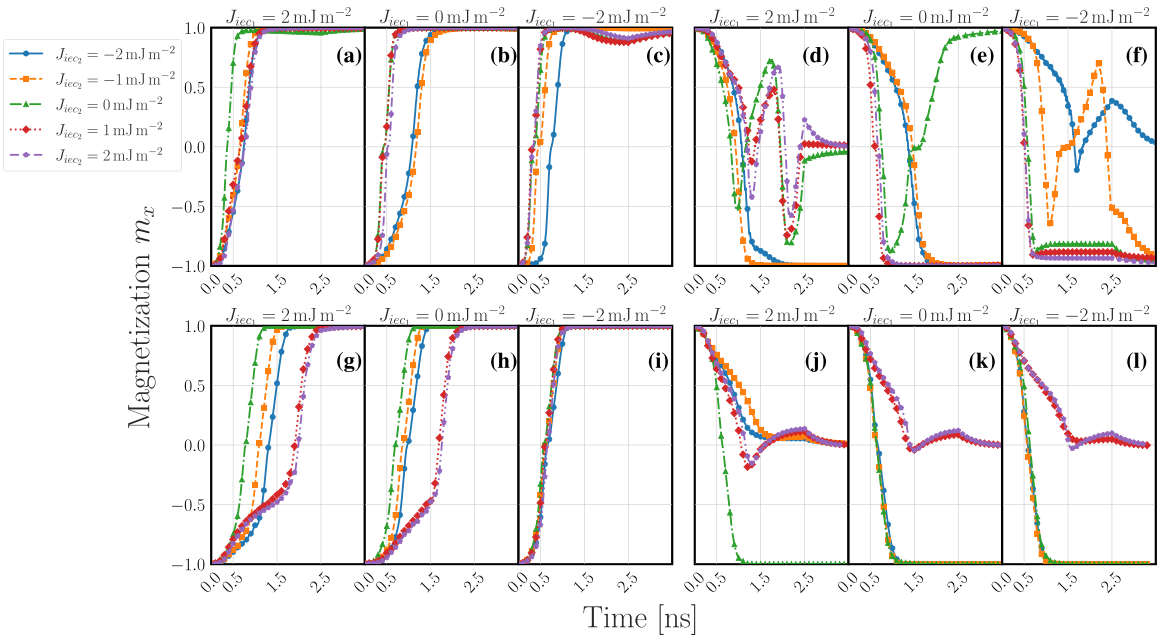

Fig. 2. Magnetization dynamics for the MRAM cells in Fig. 1, focusing on the impact of IEC strengths, J_{iec_1} and J_{iec_2}, on the switching process. **(a–c)** depict the AP to P transition, while **(d–f)** show the P to AP transition for the structure in Fig. 1(a). Likewise, **(g–l)** follow the same analysis for the structure in Fig. 1(b). The coupling strength range aligns with experimental findings on magnetic interactions. The left panel applies a negative J_{iec_1} to assess its influence on switching, the middle panel sets J_{iec_1} to zero for comparison, and the right panel introduces a positive J_{iec_1}, each case highlighting distinct switching dynamics. These simulations underscore the critical role of IEC in the switching behavior of advanced MRAM devices.

from -2 to $+2$ $\mathrm{mJ\,m^{-2}}$, were chosen to systematically explore both FM and AFM coupling regimes. These values are not intended to replicate a specific experimental configuration, but rather to capture the broader effects of IEC variability on the switching dynamics. As highlighted in previous studies [22,26], experimentally reported IEC values vary widely depending on material systems and fabrication conditions. For example, Hashimoto et al. [27] report a ferromagnetic coupling of 2 $\mathrm{mJ\,m^{-2}}$ for Ru spacers with a thickness of 0.35 nm, while McKinnon et al. [28] observe antiferromagnetic coupling as strong as -3 $\mathrm{mJ\,m^{-2}}$ for Ru spacers of 0.4 nm. These examples demonstrate that stronger IEC values can be achieved through spacer engineering. Our selected range thus ensures that the full qualitative behavior of IEC is represented in a general and transferable simulation framework.

3. Results

This section details the outcomes from switching simulations conducted on the configurations illustrated in Fig. 1. We varied the interlayer exchange coupling constant, J_{iec}, from -2 $\mathrm{mJ\,m^{-2}}$ to $+2$ $\mathrm{mJ\,m^{-2}}$. This selected range is consistent with the experimental values noted in NMS [29,30] and captures the oscillatory behavior in the TB, challenging the conventional view of dominant FM coupling [31]. Notably, some instances exhibited coupling strengths exceeding ± 2 $\mathrm{mJ\,m^{-2}}$ [32].

Fig. 2(a–c) illustrates the magnetization trajectories as they shift from AP to P alignment, as seen in Stack A of Fig. 1(a). We explore the effects of varying J_{iec_1} and J_{iec_2} on the dynamics of switching. Here, J_{iec_1} is the coupling strength between the RL and the first free layer ($\mathrm{FL_1}$), and J_{iec_2} is the coupling strength between $\mathrm{FL_1}$ and the second free layer ($\mathrm{FL_2}$). In Fig. 2(a), J_{iec_1} is kept constant at -2 $\mathrm{mJ\,m^{-2}}$ while J_{iec_2} is adjusted. The condition where $J_{iec_1} = -2$ $\mathrm{mJ\,m^{-2}}$ and $J_{iec_2} = 0$ results in the fastest switching, due to the absence of coupling between $\mathrm{FL_1}$ and $\mathrm{FL_2}$. Surprisingly, this lack of coupling enables $\mathrm{FL_2}$ to switch more swiftly, independent of whether the existing coupling with $\mathrm{FL_1}$ is FM or AFM.

In Fig. 2(b), where $J_{iec_1} = 0$, a relevant contrast is observed. As $\mathrm{FL_1}$ begins its precessional movement, the AFM coupling ($J_{iec_2} < 0$) between $\mathrm{FL_1}$ and $\mathrm{FL_2}$ leads to dynamic interlayer coupling, slowing the switching process. This interaction encourages a more uniform magnetization reversal without the typical plateau at $m_x = 0$, unlike scenarios where $J_{iec_2} \geq 0$. The absence of direct coupling between the RL and $\mathrm{FL_1}$ allows relatively rapid switching at moderate coupling strengths. However, at the maximum coupling values (± 2 $\mathrm{mJ\,m^{-2}}$), the switching rate decreases. For FM coupling, stronger interactions strive to keep $\mathrm{FL_1}$ and $\mathrm{FL_2}$ in P alignment, thus slowing the process compared to weaker FM coupling scenarios. Conversely, in AFM coupling, the stronger interaction coupled with dynamic interlayer effects prompts an earlier reversal in $\mathrm{FL_2}$, resulting in faster switching than with intermediate AFM strengths.

Fig. 2(c) shows that when the coupling between the RL and $\mathrm{FL_1}$ is ferromagnetic ($J_{iec_1} > 0$), the fastest switching occurs under the strongest J_{iec_2}. This observation underscores the complex interplay between the magnetic layers and highlights the critical impact of IEC on the dynamics of multilayer magnetic systems.

Fig. 2(d–f) demonstrate the magnetization trajectories during transitions from P to AP alignment. Fig. 2(d) keeps J_{iec_1} constant at -2 $\mathrm{mJ\,m^{-2}}$ while varying J_{iec_2}. Here, only AF coupling at J_{iec_2} enables successful switching, emphasizing the critical role of IEC in multilayer structures. A write error occurs if $J_{iec_2} \geq 0$. Initially, the field-like and damping-like torques act in conjunction. However, once the FLs reverse, these torques begin to counteract each other. The IEC between the layers plays a crucial role in this process, either supporting or hindering back-hopping, as illustrated in Fig. 4 and Fig. 5 in [33].

For all simulations, the bias is turned off at 2.5 ns to allow the system to relax. In the cases shown in Fig. 2(a–c) and (g–i), the system relaxes to the desired final magnetization configuration, confirming stable switching. However, in Fig. 2(d) and Fig. 2(f), the system does not settle into a complete AP state. Instead, it relaxes into an intermediate configuration around $m_x = 0$, which reflects an AP alignment between the two FLs.

One way to mitigate back-hopping and improve STT efficiency is to use the IEC itself. As shown in our results, properly tuned AFM IEC can help stabilize the final magnetic state and suppress back transitions by enforcing alignment between the layers.

A second approach is to engineer structural asymmetry in the MTJ stack. As demonstrated by Manchon et al. [34], breaking inversion symmetry modifies the bias dependence of spin torque, which can reduce stochastic switching behavior. Similarly, Oh et al. [35] showed that asymmetries in material composition and bias conditions affect the magnetic phase stability. By carefully selecting materials and layer thicknesses, it is possible to expand the stability region of the parallel configuration and further suppress back-hopping.

Fig. 2(g–l) follow the same setup as Fig. 2(a–f), but for Stack B. Regarding the relationship to double spin torque magnetic tunnel junction (ds-MTJ), we note that the configuration shown in Fig. 1(b) bears similarity to a ds-MTJ. In a typical ds-MTJ, the second magnetic layer on the opposite side of the FL acts as a second reference layer (RL_2) with fixed magnetization, contributing to additional spin torque. In contrast, in our setup, the corresponding layer (FL_2) is not fixed, but is itself a FL. Although the initial antiparallel alignment and subsequent inversion of FL_2 resemble the magnetization structure of a ds-MTJ during switching, the key difference is that FL_2 is dynamic rather than static. Additionally, the choice of the NMS material and its associated spin flip length plays a crucial role in torque transmission. For example, tungsten ($\lambda_{sf} = 2.4$ nm) causes a stronger spin torques than tantalum ($\lambda_{sf} = 1.9$ nm). These spin transport properties of the NMS significantly influence torque distribution and switching dynamics. The presence of IEC further adds to the complexity by coupling the layers and modifying the overall torque landscape. Fig. 2(g) documents the condition, where $J_{iec_1} = -2\ \mathrm{mJ\,m^{-2}}$ and $J_{iec_2} = 0$ leads to the fastest switching due to the absence of coupling between FL_1 and FL_2. This lack of coupling allows for swift switching of FL_2, regardless of its coupling nature with FL_1, whether FM or AFM.

In Fig. 2(h), where $J_{iec_1} = 0$, the magnetization in FL_1 begins its precessional movement, and the AFM coupling ($J_{iec_2} < 0$) with FL_2 leads to dynamic interlayer coupling which slows down the switching process. This results in a longer delay before reversal occurs, attempting to maintain the P alignment between FL_1 and FL_2.

The absence of direct coupling between the RL and FL_1 promotes relatively rapid switching. However, at the highest coupling values ($\pm 2\ \mathrm{mJ\,m^{-2}}$), the switching process is slowed. In cases of FM coupling, stronger interactions strive to keep FL_1 and FL_2 in P alignment, slowing the process compared to weaker FM coupling. Conversely, in AFM coupling, stronger interactions and dynamic effects prompt an earlier reversal in FL_2, resulting in faster switching than with intermediate AFM strengths.

The transient behavior shown in Fig. 2(g) and 2(h) results from the positive J_{iec_2}, which favors P alignment between FL_1 and FL_2, making their relative rotation more constrained and the switching process more challenging. When the magnetizations are collinear, either P or AP, the spin transfer torque is minimal due to the small angle between them, limiting its ability to effectively drive the transition.

Fig. 2(j) shows that when the coupling between the RL and FL_1 is FM ($J_{iec_1} > 0$), variations in J_{iec_2} play a less significant role. This highlights the complex interactions between the magnetic layers and emphasizes the significant influence of IEC on the dynamics of multilayer magnetic systems.

Fig. 2(k) illustrates the magnetization trajectories during the transition from P to AP alignment. As in the previous figure, Fig. 2(j) maintains J_{iec_1} at $-2\ \mathrm{mJ\,m^{-2}}$ while J_{iec_2} is varied. Here, successful switching occurs only, when there is no coupling ($J_{iec_2} = 0$), showcasing the critical role of IEC in multilayer structures. Any nonzero J_{iec_2} leads to write errors.

Similar to earlier discussions, Fig. 2(k) indicates that successful switching occurs with $J_{iec_2} \geq 0$. However, if the coupling between FL_1 and FL_2 ($J_{iec_2} \leq 0$) persists, it leads to write errors. This is attributed to the coupling maintaining the inverted magnetization of FL_2. Fig. 2(l) offers a similar depiction, emphasizing the importance of the correct IEC configuration to avoid write errors.

The interface-induced uniaxial anisotropy defines a preferred direction for the magnetization of the FL, which in this setup is aligned along the positive x-direction. This anisotropy energetically favors magnetization alignment along that axis. At the same time, stray magnetic fields originating from the fixed magnetic layer promote a P alignment of the magnetic moments. Together, these internal contributions stabilize the P magnetic configuration and bias the system toward it. As a result, the transitions between the AP and P states become asymmetric: switching from the AP to the P state is energetically favored and occurs more easily, while switching from the P to the AP state requires overcoming a higher energy barrier. This asymmetry is observed in both magnetic tunnel junction designs.

4. Conclusion

Our study investigates the dynamics of multilayer magnetic systems through switching simulations under varying IEC conditions, contributing to the advancement of spintronic research. By tuning the interlayer exchange coupling constant within experimentally validated ranges, we demonstrate how IEC influences magnetization trajectories and switching behavior beyond conventional ferromagnetic assumptions.

Specific IEC configurations were shown to significantly accelerate switching, emphasizing the potential of tailored IEC to enhance device performance. Moreover, the role of dynamic interlayer coupling in achieving uniform magnetization reversal and suppressing write errors highlights the importance of precisely engineered coupling strengths for reliable and efficient operation.

These findings challenge traditional perspectives on magnetic coupling in multilayer stacks and open pathways to leverage IEC for improved functionality in spintronic devices. Fine-tuning IEC parameters may enable faster write/read operations and better data retention, which is critical for the continued scaling and efficiency of nanoscale memory technologies. As such, this work offers considerable insights for both fundamental understanding and practical optimization in magnetic memory design.

CRediT authorship contribution statement

M. Bendra: Writing – review & editing, Writing – original draft, Visualization, Software, Methodology, Investigation, Data curation, Conceptualization. **R.L. de Orio:** Writing – review & editing, Software. **S. Selberherr:** Writing – review & editing, Supervision, Resources, Funding acquisition. **W. Goes:** Writing – review & editing, Supervision, Resources. **V. Sverdlov:** Writing – review & editing, Supervision, Project administration, Funding acquisition, Conceptualization.

Declaration of competing interest

The authors declare that they have no known competing financial interests or personal relationships that could have appeared to influence the work reported in this paper.

Acknowledgments

The financial support by the Federal Ministry of Economy, Energy and Tourism, the National Foundation for Research, Technology, and Development, the Christian Doppler Research Association, Austria, and the TU Wien Library, Austria for financial support through its Open Access Funding Program is gratefully acknowledged.

Data availability

Data will be made available on request.

References

[1] Jung S, Lee H, Myung S, Kim H, Yoon SK, et al. A crossbar array of magnetoresistive memory devices for in-memory computing. Nature 2022;601:211–6. http://dx.doi.org/10.1038/s41586-021-04196-6.

[2] Naik VB, Yamane K, Lee T, Kwon J, Chao R, et al. JEDEC-qualified highly reliable 22nm FD-SOI embedded MRAM for low-power industrial-grade, and extended performance towards automotive-grade-1 applications. In: IEEE international electron devices meeting. 2020, p. 11.3.1–4. http://dx.doi.org/10.1109/IEDM13553.2020.9371935.

[3] Ikegawa S, Nagel K, Mancoff FB, Alam SM, Arora M, et al. High-speed (400MB/s) and low-BER STT-MRAM technology for industrial applications. In: IEEE international electron devices meeting. 2022, p. 10.4.1–4. http://dx.doi.org/10.1109/IEDM45625.2022.10019513.

[4] Gebregiorgis A, Wu L, Münch C, Rao S, Tahoori MB, Hamdioui S. Special session: STT-MRAMs: Technology, design and test. In: 2022 IEEE 40th VLSI test symposium. 2022, p. 1–10. http://dx.doi.org/10.1109/VTS52500.2021.9794278.

[5] Igarashi J, Jinnai B, Watanabe K, Shinoda T, Funatsu T, Sato H, et al. Single-nanometer CoFeB/MgO magnetic tunnel junctions with high-retention and high-speed capabilities. Npj Spintron 2024;2:211–6. http://dx.doi.org/10.1038/s44306-023-00003-2.

[6] Phoomatna R, Sampan-a-pai S, Meo A, Chantrell RW, Chureemart J, Chureemart P. Dimensional scaling effects on critical current density and magnetization switching in CoFeB-based magnetic tunnel junction. J Phys D: Appl Phys 2024;57(18):185002. http://dx.doi.org/10.1088/1361-6463/ad2477.

[7] Abert C, Sepehri-Amin H, Bruckner F, Vogler C, Hayashi M, Suess D. Back-hopping in spin-transfer-torque devices: Possible origin and countermeasures. Phys Rev Appl 2018;9. http://dx.doi.org/10.1103/PhysRevApplied.9.054010.

[8] Kumar Yadav M, Kumar R, Kumar Ratnesh R, Singh J, Chandra R, Kumar A, et al. Revolutionizing technology with spintronics: Devices and their transformative applications. Mater Sci Eng: B 2024;303:117293. http://dx.doi.org/10.1016/j.mseb.2024.117293.

[9] Sato H, Yamanouchi M, Ikeda S, Fukami S, Matsukura F, Ohno H. MgO/CoFeB/Ta/CoFeB/MgO recording structure in magnetic tunnel junctions with perpendicular easy axis. In: IEEE transactions on magnetics. 49, 2013, p. 4437–40. http://dx.doi.org/10.1109/TMAG.2013.2251326.

[10] Jinnai B, Igarashi J, Watanabe K, Funatsu T, Sato H, et al. High-performance shape-anisotropy magnetic tunnel junctions down to 2.3 nm. In: IEEE international electron devices meeting. 2020, p. 24.6.1–4. http://dx.doi.org/10.1109/IEDM13553.2020.9371972.

[11] Cai W, Wang M, Cao K, Yang H, Peng S, et al. Stateful implication logic based on perpendicular magnetic tunnel junctions. In: Sci. China inf. sci., vol. 65, 2022, 122406. http://dx.doi.org/10.1007/s11432-020-3189-x.

[12] Ikeda S, Miura K, Yamamoto H, Mizunuma K, Gan HD, et al. A perpendicular-anisotropy CoFeB–MgO magnetic tunnel junction. In: Nature materials, vol. 9, 2010, p. 721–4. http://dx.doi.org/10.1038/nmat2804.

[13] Lepadatu S. Boris computational spintronics online materials database. 2024, http://www.boris-spintronics.uk/online-materials-database/. [Accessed 24 March 2024].

[14] Kolev T, Dobrev V. MFEM: Modular finite element methods library. 2024, http://mfem.org. [Accessed 24 March 2024].

[15] ViennaSpinMag. An open access finite element-based application for calculating the magnetization dynamics of multi-layered structures composed of ferromagnets, metal spacers and tunnel barriers. 2024, https://www.iue.tuwien.ac.at/viennaspinmag/. [Accessed 24 March 2024].

[16] Fiorentini S, Bendra M, Ender J, de Orio RL, Goes W, Selberherr S, et al. Spin and charge drift-diffusion in ultra-scaled MRAM cells. Sci Rep 2022;12:20958. http://dx.doi.org/10.1038/s41598-022-25586-4.

[17] Ender J, Mohamedou M, Fiorentini S, Orio R, Selberherr S, Goes W, et al. Efficient demagnetizing field calculation for disconnected complex geometries in STT-MRAM cells. In: 2020 international conference on simulation of semiconductor processes and devices. 2020, p. 213–6. http://dx.doi.org/10.23919/SISPAD49475.2020.9241662.

[18] Miltat JE, Donahue MJ. Numerical micromagnetics: Finite difference methods. In: Handbook of magnetism and advanced magnetic materials. Micromagnetism, John Wiley & Sons, Ltd; 2007, http://dx.doi.org/10.1002/9780470022184.hmm202.

[19] Ruderman MA, Kittel C. Indirect exchange coupling of nuclear magnetic moments by conduction electrons. Phys Rev 1954;96:99–102. http://dx.doi.org/10.1103/PhysRev.96.99.

[20] Inomata K, Yusu K, Saito Y. Magnetoresistance associated with antiferromagnetic interlayer coupling spaced by a semiconductor in Fe /Si multilayers. Phys Rev Lett 1995;74:1863–6. http://dx.doi.org/10.1103/PhysRevLett.74.1863.

[21] Bruno P. Theory of interlayer exchange interactions in magnetic multilayers. J Phys: Condens Matter 1999;11(48):9403–19. http://dx.doi.org/10.1088/0953-8984/11/48/305.

[22] Flauger P, Abert C, Suess D. Computational assessment of possible origins of the back-hopping effect in magnetic tunnel junctions. Phys Rev B 2023;108:014430. http://dx.doi.org/10.1103/PhysRevB.108.014430.

[23] Abert C. Micromagnetics and spintronics: models and numerical methods. Eur Phys J B 2019;92(6):120. http://dx.doi.org/10.1140/epjb/e2019-90599-6.

[24] Fiorentini S, Jørstad NP, Ender J, de Orio RL, Selberherr S, Bendra M, et al. Finite element approach for the simulation of modern MRAM devices. Micromachines 2023;14(5). http://dx.doi.org/10.3390/mi14050898.

[25] Bendra M, Orio RLd, Selberherr S, Goes W, Sverdlov V. Advanced modeling and simulation of multilayer spin–transfer torque magnetoresistive random access memory with interface exchange coupling. Micromachines 2024;15(5). http://dx.doi.org/10.3390/mi15050568.

[26] Bin Hamid S, Dutta R, Hassan O, Baten MZ. Implementing bidirectional logic with backhopping in magnetic tunnel junctions. AIP Adv 2024;14(2):025224. http://dx.doi.org/10.1063/5.0169751.

[27] Hashimoto A, Saito S, Kim D, Takashima H, Ueno T, Takahashi M. Fe content dependence of synthetic-antiferromagnetic coupling in subnano-crystalline FeCoB/Ru/FeCoB films. IEEE Trans Magn 2006;42(10):2342–4. http://dx.doi.org/10.1109/TMAG.2006.879432.

[28] McKinnon T, Heinrich B, Girt E. Spacer layer thickness and temperature dependence of interlayer exchange coupling in Co/Ru/Co trilayer structures. Phys Rev B 2021;104:024422. http://dx.doi.org/10.1103/PhysRevB.104.024422.

[29] Khodadadi B, Mohammadi JB, Jones JM, Srivastava A, Mewes C, Mewes T, et al. Interlayer exchange coupling in asymmetric Co–Fe/Ru/Co–Fe trilayers investigated with broadband temperature-dependent ferromagnetic resonance. Phys Rev Appl 2017;8:014024. http://dx.doi.org/10.1103/PhysRevApplied.8.014024.

[30] Mouhoub A, Millo F, Chappert C, Kim J-V, Létang J, Solignac A, et al. Exchange energies in CoFeB/Ru/CoFeB synthetic antiferromagnets. Phys Rev Mater 2023;7:044404. http://dx.doi.org/10.1103/PhysRevMaterials.7.044404.

[31] Weng Y-C, Cheng C-W, Chern G. Interlayer exchange coupling and perpendicular magnetic anisotropy in $Co_{40}Fe_{40}B_{20}$/MgO/$Co_{20}Fe_{60}B_{20}$ tunnel junction structures. IEEE Trans Magn 2013;49:4425–8. http://dx.doi.org/10.1109/TMAG.2013.2245308.

[32] Katayama T, Yuasa S, Velev J, Zhuravlev MY, Jaswal SS, Tsymbal EY. Interlayer exchange coupling in Fe/MgO/Fe magnetic tunnel junctions. Appl Phys Lett 2006;89(11):112503. http://dx.doi.org/10.1063/1.2349321.

[33] Bendra M, de Orio R, Selberherr S, Goes W, Sverdlov V. A multi-level cell for ultra-scaled STT-MRAM realized by back-hopping. Solid-State Electron 2025;223:109027. http://dx.doi.org/10.1016/j.sse.2024.109027.

[34] Manchon A, Zhang S, Lee K-J. Signatures of asymmetric and inelastic tunneling on the spin torque bias dependence. Phys Rev B 2010;82:174420. http://dx.doi.org/10.1103/PhysRevB.82.174420.

[35] Oh S-C, Park S-Y, Manchon A, Chshiev M, Han J-H, et al. Bias-voltage dependence of perpendicular spin-transfer torque in asymmetric MgO-based magnetic tunnel junctions.